ACS OMEGA

Open Access

http://pubs.acs.org/journal/acsodf

Article

Adsorption Mechanism and Regeneration Performance of Calcined Zeolites for Hydrogen Sulfide and Its Application

Xianghao Zha, Feixing Li, Bo Feng, Xin Zhang, and Ruo He*

Cite This: *ACS Omega* 2024, 9, 19493−19503

Read Online

ACCESS | Metrics & More | Article Recommendations

ABSTRACT: Hydrogen sulfide (H_2S) is a very toxic, acidic, and odorous gas. In this study, a calcined zeolite was used to investigate the adsorption performance of H_2S. Among particle size, calcination temperature and time calcination temperature and time had significant effects on the adsorption capacity of H_2S on the zeolite. The optimal calcination conditions for the zeolite were 332 °C, 1.8 h, and 10−20 mm size, and the maximum adsorption capacity of H_2S was approximately 6219 mg kg^{-1}. Calcination could broaden the channels, remove the adsorbed gases and impurities on the surface of zeolites, and increase the average pore size and point of zero net charge. As the zeolite adsorbed to saturation, it could be regenerated at the temperatures between 200 and 350 °C for 0.5 h. Compared with the natural zeolite, the adsorption capacities of dimethyl disulfide, dimethyl sulfide, toluene, CH_3SH, CS_2, CO_2, and H_2S were significantly higher on the calcined zeolite, while the adsorption capacity of CH_4 was lower on the calcined zeolite. A gas treatment system by a temperature swing adsorption−regeneration process on honeycomb rotors with calcined zeolites was proposed. These findings are helpful for developing techniques for removing gas pollutants such as volatile sulfur compounds and volatile organic compounds to purify biogas and to limited toxic concentrations in the working environment.

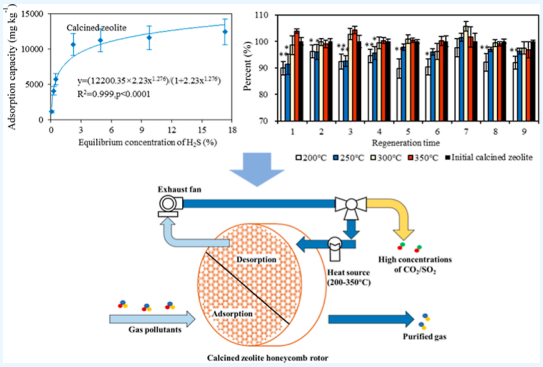

1. INTRODUCTION

Hydrogen sulfide (H_2S) is a very toxic and acidic gas. H_2S has no color, but it has a strong odor of rotten eggs, with a low odor threshold value of ∼ 0.5 ppbv.[1] H_2S is the main odorous gas generated from various waste treatment plants, such as landfills and municipal and agricultural waste compost plants, with concentrations from several to thousand parts per million by volume (ppmv).[2,3] In waste disposal plants that receive waste containing high levels of sulfur (e.g., construction and demolition debris), the H_2S concentration can reach 5−10%.[4] Industrial activities, such as wastewater treatment, paper mills and petroleum/natural gas drilling and refining, can produce H_2S as a byproduct.[5−7] H_2S can corrode transport lines and poison catalysts even at low levels in industries, such as biogas, natural gas and liquefied petroleum gas.[8] In addition, H_2S can irritate the human cornea and respiratory mucosa and cause conjunctivitis and upper respiratory tract diseases.[9] When H_2S enters the blood, it can combine with hemoglobin to form irreducible sulfurized hemoglobin and cause symptoms of poisoning.[10] Long-term exposure to low concentrations of H_2S may cause headache, fatigue, memory loss, insomnia, chest pain, cough, nausea, and diarrhea.[11,12] Therefore, in a working environment, H_2S should be removed to a level that is below the limited toxic concentration of 10 ppm.[13]

Adsorption is a common method for H_2S treatment. The main adsorbents for H_2S removal include activated carbon, bentonite, zeolite, metal oxides, and microporous polymer materials.[14−16] Of these adsorbents, activated carbon has been reported to be an effective adsorbent that can catalyze and accelerate H_2S-oxidation to elemental sulfur at room temperature and remove it by adsorption.[14] Bouzaza et al.[17] found that H_2S removal by activated carbon fibers mainly consists of physical adsorption and chemical oxidation, which are greatly affected by the humidity of the environment. Mescia et al.[18] reported that two kinds of activated carbons could significantly improve the H_2S adsorption capacity due to the different effects of the various activated carbons on H_2S removal. Although the removal of H_2S with activated carbon has been widely studied, the treatment cost is relatively high due to the limited adsorption capacity of activated carbon. Compared with activated carbon, zeolites including natural zeolites and zeolites modified by metals or metal oxides have been reported to be less expensive adsorbents for H_2S removal.[19] However, the regeneration of metal-oxide-based sorbents is usually

Received: January 31, 2024
Revised: April 3, 2024
Accepted: April 4, 2024
Published: April 16, 2024

performed at a high temperature (>400 °C), which consumes additional energy. Recently, metal−organic frameworks (MOFs) have been reported to capture and remove H_2S.[20] However, the framework of some MOFs such as MOF-199 is easily collapsed after H_2S adsorption, which is adverse to H_2S adsorption.[21] Therefore, a sorbent that is inexpensive, easily available, and regenerated is more feasible and beneficial for H_2S removal during waste disposal and industrial activities.

In this study, the effect of the zeolite particle size, calcination temperature, and calcination time was investigated to optimize the zeolite for H_2S removal. The surface morphology, surface area, pore size, X-ray diffraction (XRD) pattern, and point of zero net charge (pH_{PZNC}) of zeolite were characterized before and after calcination, and the adsorption isotherm and regeneration conditions were analyzed. Additionally, the adsorption capacities of the gas pollutants generated from waste disposal, such as CH_3SH, dimethyl disulfide, dimethyl sulfide (DMS), toluene, CS_2, CO_2, and CH_4, were determined. These results provided a deep understanding of the characteristics of H_2S adsorption on the calcined zeolite and were helpful for developing techniques for gas pollutant treatment.

2. MATERIALS AND METHODS

2.1. Experimental Materials. The zeolite used in this study was Yusong clinoptilolite, which was purchased from Gongyi city. The main physicochemical characteristics of the experimental zeolite were as follows: specific gravity, 2.16 g cm^{-3}; volume weight, 1.35 g cm^{-3}; mud content, ≤1.0%; ammonia absorption capacity, 1.5−1.6 mmol g^{-1}; SiO_2, 68−71%; Al_2O_3, 13−14%; Fe_2O_3, 1−1.8%; CaO, 1.8−2.2%; MgO, 0.9−1.4%; K_2O, 1.6−3.9%; NaO, 0.6−1.6% (Table 1). After being washed and air-dried, the zeolite was sieved into three particle sizes, that is, 4−6, 6−10, and 10−20 mm.

Table 1. Main Physicochemical Properties of the Experimental Zeolite

parameter	value	parameter	value
solubility in hydrochloric acid solution	≤2.26%	ammonia absorption capacity	1.5−1.6 mmol g^{-1}
specific gravity	2.16 g cm^{-3}	SiO_2	68−71%
volume weight	1.35 g cm^{-3}	Al_2O_3	13−14%
wear rate	≤0.8%	Fe_2O_3	1−1.8%
crashed rate	≤1.0%	CaO	1.8−2.2%
porosity	≥56%	MgO	0.9−1.4%
mud content	≤1.0%	K_2O	1.6−3.9%
moisture content	≤1.8%	NaO	0.6−1.6%

2.2. Batch Experiment of Calcined Zeolite for H_2S Removal. *2.2.1. Zeolite Particle Size.* Three particle sizes of the zeolite, including 4−6, 6−10, and 10−20 mm, were used to determine the effect of zeolite particle size on H_2S adsorption. The calcination condition of the zeolite was set at 400 °C for 2 h.

2.2.2. Calcination Temperature. Based on the experimental results of the zeolite particle size, the optimal zeolite particle size was used for this test. To determine the effect of calcination temperature on H_2S adsorption, the experiment was performed at 150, 200, 300, 400, 500, and 600 °C with a calcination time of 2 h.

2.2.3. Calcination Time. Based on the experimental results of the calcination temperature and particle size, the optimal zeolite particle size and calcination temperature were studied further. The time was set at 0.5, 1, 1.5, 2, 2.5, and 3 h to determine the effect of the zeolite calcination time on H_2S adsorption.

2.2.4. Box−Behnken Experiment. Based on the experimental results of a single factor including the zeolite particle size, calcination temperature, and time, a Box-Behnken experiment of particle size (4−6, 6−10, and 10−20 mm), calcination temperature (200, 400, and 600 °C) and calcination time (1, 2, and 3 h) was designed to optimize the calcination conditions of the zeolite.

Approximately 4 g of natural zeolite or calcined zeolite was placed in 160 mL serum bottles for the above batch tests (unless stated otherwise). The serum bottles were flushed with high purity N_2 (99.999%) at a flow rate of 200 mL min^{-1} for 5 min and then sealed with a butyl rubber stopper. After extraction of a certain amount of gas from the serum bottles, H_2S was injected to achieve a concentration of 10% (v/v) in the headspace. A treatment without zeolite was used as a control. Each treatment was performed in triplicate. All serum bottles were placed at 30 °C. Gas samples were collected from the headspace of the serum bottles to measure the H_2S concentration after 12 h (a preliminary experiment showed that the adsorption equilibrium of H_2S was obtained within 6−12 h).

2.3. Analysis of Physicochemical Properties. The structural properties of the zeolite were characterized using an X'pert PRO X-ray diffractometer (Netherlands, Panaco) with CuKα radiation (λ = 1.54 Å) in a 2θ range of 8−35° at a step size of 0.02°. The working voltage and current were 40 kV and 40 mA, respectively. The surface area and pore size properties of the zeolite were analyzed at 77.35 K (liquid nitrogen temperature) by an Autosorb-1-C ratio surface area and pore size distribution apparatus (Quantachrome instruments, USA). Any adsorbed gases or vapors were removed before the actual measurement by being degassed at 120 °C for 24 h. Then, the samples were vacuumed at 5.0 cm^3 g^{-1} with nitrogen as the adsorbate. The surface area and pore size were calculated as described previously.[22] The zeolite morphology was analyzed before and after calcination by using cold field emission scanning electron microscopy (SEM) (SU8010 Hitachi, Japan). The pH_{PZNC} value of the zeolite was determined using the titration method as described previously.[23] In brief, 25 mL of a 0.001 mol L^{-1} $NaNO_3$ solution with pH values of 2, 4, 6, 8, 10, or 12 was added into a flask, and then the zeolite was added to obtain the contents at 40, 80, 120, 160, 200, and 300 g L^{-1}. After the solution was shaken at 150 rpm and 30 °C for 24 h, the pH value of the solution was determined.

2.4. Adsorption Isotherm and Regeneration of Zeolite. The adsorption isotherm of H_2S was determined in the H_2S concentration range of 0.1 to 17% (v/v). Approximately 4 g of calcined zeolite or natural zeolite was placed in 160-mL serum bottles, and H_2S was injected to obtain the setting concentrations. Gas samples were periodically collected from the headspace of the serum bottles to measure the H_2S concentration until adsorption equilibrium (12 h).

The H_2S-saturated zeolite was regenerated at temperatures of 200, 250, 300, and 350 °C for 0.5 h. A treatment without zeolite was used as a control. Five replicates were established

https://doi.org/10.1021/acsomega.4c00987
ACS Omega 2024, 9, 19493−19503

for each treatment. Gas samples were collected from the headspace of the serum bottles to measure H_2S concentration after 12 h. The regeneration test was repeated ninetimes.

Each treatment of the zeolite adsorption isotherm and regeneration was performed by the same method as described in the batch experiments (unless stated otherwise).

2.5. Analysis of the Adsorption Capacity. The adsorption capacities of CH_3SH, dimethyl disulfide, toluene, DMS, CS_2, CO_2, and CH_4 on the calcined zeolite or natural zeolite were tested. The experiment was performed in 160-mL serum bottles by the same method as described in the batch experiments. After extracting a certain amount of gas from the headspace of the serum bottles, CH_3SH, dimethyl disulfide, toluene, DMS, and CS_2 were injected to obtain a concentration of 2000 ppm (v/v), and CO_2 and CH_4 were injected to 10% (v/v). After 12 h, gas samples were collected from the headspace of the serum bottles to measure CH_3SH, dimethyl disulfide, toluene, DMS, CS_2, CO_2, and CH_4.

The concentrations of H_2S, CH_3SH, dimethyl disulfide, DMS, and CS_2 were measured using an HC-3-trace sulfur analyzer.[24] The toluene concentration was determined as described by Su et al.[25] The concentrations of CH_4 and CO_2 were analyzed by using gas chromatography equipped with a thermal conductivity detector as described previously.[26] The adsorption capacity of gas, including H_2S, CH_3SH, dimethyl disulfide, DMS, CS_2, CH_4, and CO_2, was calculated by using the following equation.

$$Q_e = \frac{273M[(c_0 - c_e) - (c_{k0} - c_{ke})]v \times 10^{-6}}{22.4Tm} \quad (1)$$

where Q_e is the adsorption capacity of gas on the zeolite, mg kg^{-1}; M is the molar mass of gas, $g\ mol^{-1}$; 273 is the standard Kelvin temperature (0 °C), K; c_0 is the initial concentration of gas in the headspace of the experimental serum bottle, ppmv; c_e is the gas concentration in the headspace at time t, ppmv; c_{k0} is the initial concentration of gas in the control, ppmv; c_e is the gas concentration in the control at time t, ppmv; v is the volume of the serum, L; 22.4 is the standard volume of 1 mol of an ideal gas at standard temperature and pressure, L mol^{-1} K^{-1}; T is the experimental temperature, K; and m is the dry mass of zeolite, kg.

3. RESULTS AND DISCUSSION

3.1. Effect of Zeolite Calcination Conditions on H_2S Adsorption. In this study, calcination conditions, including zeolite particle size, calcination temperature, and time, were investigated to optimize H_2S adsorption removal by the zeolite (Figure 1). The adsorption capacity of H_2S was 3202 ± 102, 2858 ± 55, and 1872 ± 51 mg kg^{-1} on the natural zeolites with sizes of 4−6, 6−10, and 10−20 mm, respectively, which only accounted for 28.9−53.3% of the calcined zeolite of the corresponding particle size, indicating that the calcined zeolite could significantly enhance H_2S adsorption. This result might be attributed to the removal of moisture, volatile compounds and other impurities from the cavity and pore of the calcined zeolite.[27] With the increase of particle size, the adsorption capacity of H_2S on the natural zeolite decreased, likely due to the decrease of the surface area.[28] However, the adsorption capacity of H_2S on the calcined zeolite was similar, and all of the adsorption capacities reached above 6000 mg kg^{-1} at the examined particle sizes.

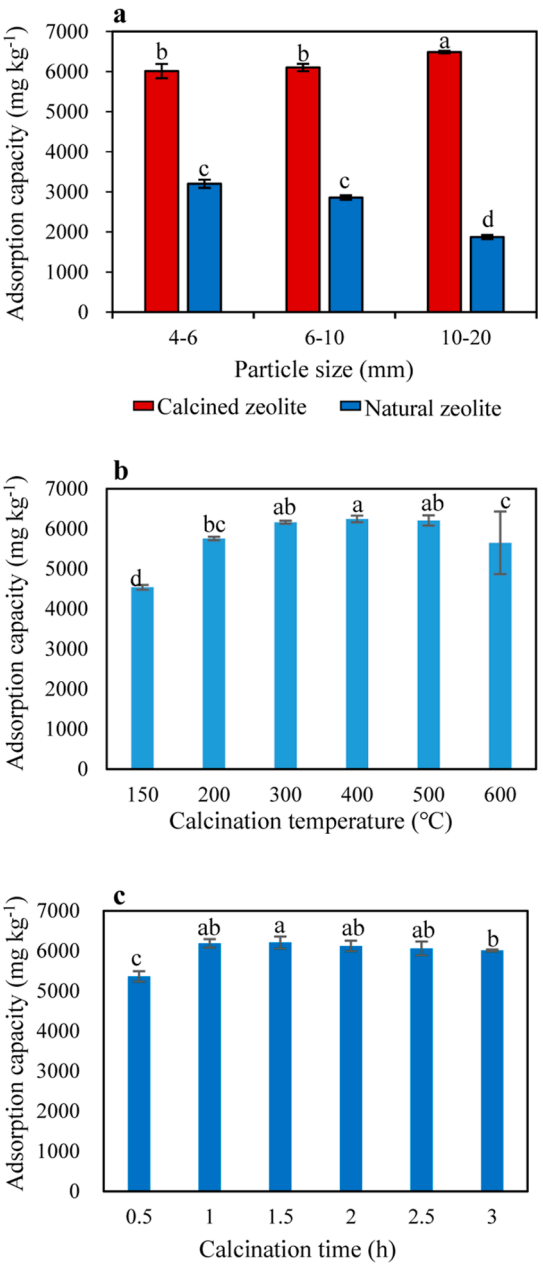

Figure 1. Effects of particle size (a), calcination temperature (b) calcination time (c) on the adsorption capacity of H_2S on the natural zeolite and calcined zeolite. Different small letter(s) means significant difference at $p < 0.05$.

The adsorption capacity of H_2S on the calcined zeolite increased when the calcination temperature increased from 200 to 400 °C and then decreased between 400 and 600 °C. The optimal calcination temperature for the zeolite was approximately 400 °C. The effect of the zeolite calcination temperature on the adsorption capacity of H_2S might be attributed to the high removal of residual water and impurities with increasing calcination temperature, which increased the surface pore size of the zeolite and facilitated the diffusion of H_2S into the zeolite.[29] When the calcination temperature was 200 and 600 °C, the adsorption capacity of H_2S on the calcined zeolite was 5757 and 5651 mg kg^{-1}, respectively, which were both lower than the adsorption capacity of H_2S on the calcined zeolite at 300, 400 and 500 °C. This decrease in

https://doi.org/10.1021/acsomega.4c00987
ACS Omega 2024, 9, 19493−19503

the adsorption capacity of H_2S might be mainly attributed to two reasons: (1) the uncompleted removal of impurities, such as residual water and volatile compounds, in zeolites at the low calcination temperature;[28] and (2) the sinter, lattice collapse and channel overlap of the zeolite at the high calcination temperature.[30]

As the calcination time increased, the adsorption capacity of H_2S on the zeolite increased and reached a maximum of 6210 mg kg^{-1} at a calcination time of 1.5 h. There was no significant difference in the adsorption capacity of H_2S on the zeolite with a calcination time between 1 and 3 h, suggesting that residual impurities, such as water and volatile compounds, in the zeolite could almost be removed after calcination at 400 °C for 1 h.

Based on the single factor test including particle size, calcination temperature, and time, a Box−Behnken experiment was conducted to optimize the calcination conditions of the zeolite for H_2S adsorption. According to the design principle of the Box−Behnken experiment, a quadratic polynomial response surface model was established. The 3D response surface of the effect of particle size, calcination temperature, and time and their interaction on the adsorption capacity of H_2S is shown in Figure 2. The response surface data were statistically analyzed to obtain the quadratic multiple regression equation of the adsorption capacity of H_2S (Y) for calcination temperature (X_1), calcination time (X_2), and particle size (X_3).

$$Y = 6110.93 - 378.85X_1 - 208.32X_2 + 152.66X_3 - 365.20X_1X_2 - 14.41X_1X_3 + 75.41X_2X_3 - 616.77X_1^2 - 583.46X_2^2 + 416.26X_3^2$$

Statistical analysis showed that the adsorption capacity of H_2S on the zeolite could fit well with the quadratic multiple regression equation ($R^2 = 0.7803$). Among the three factors, the calcination temperature and calcination time had significant influences on the adsorption capacity of H_2S on the zeolite. The optimal calcination conditions for the zeolite were 332 °C, 1.8 h, and 10−20 mm, and the maximum adsorption capacity of H_2S was 6219 mg kg^{-1}.

3.2. Characterization of the Calcined Zeolite. The morphologies of the natural zeolite and calcined zeolite (calcination was run at the optimal condition obtained by the Box−Behnken experiment) were characterized by using SEM imaging (Figure 3a-b). The surface of the natural zeolite was uneven with particle distribution, and there was no collapse or cracks in the overall structure with certain holes. However, the overall channel was relatively flat and dense in the natural zeolite. The granular structure of the calcined zeolite was flat, and the surface was relatively scattered and loose, indicating that calcination could broaden the channel of zeolite and remove the adsorbed gases and impurities on the surface of zeolite. Guo et al.[31] found that calcination could change a zeolite structure by means such as crystal structure collapse, water removal, phase change, and bond rupture. When the calcination temperature was high, the crystal and surface structure of the zeolite changed significantly and even melted at 800 °C, resulting in a decrease in the active surface area.[32]

Compared with the standard diffraction pattern of natural clinoptilolite, all of the characteristic diffraction peaks of zeolite were available, and no displacement occurred at the peak point after calcination (Figure 3c). Although the skeleton structure

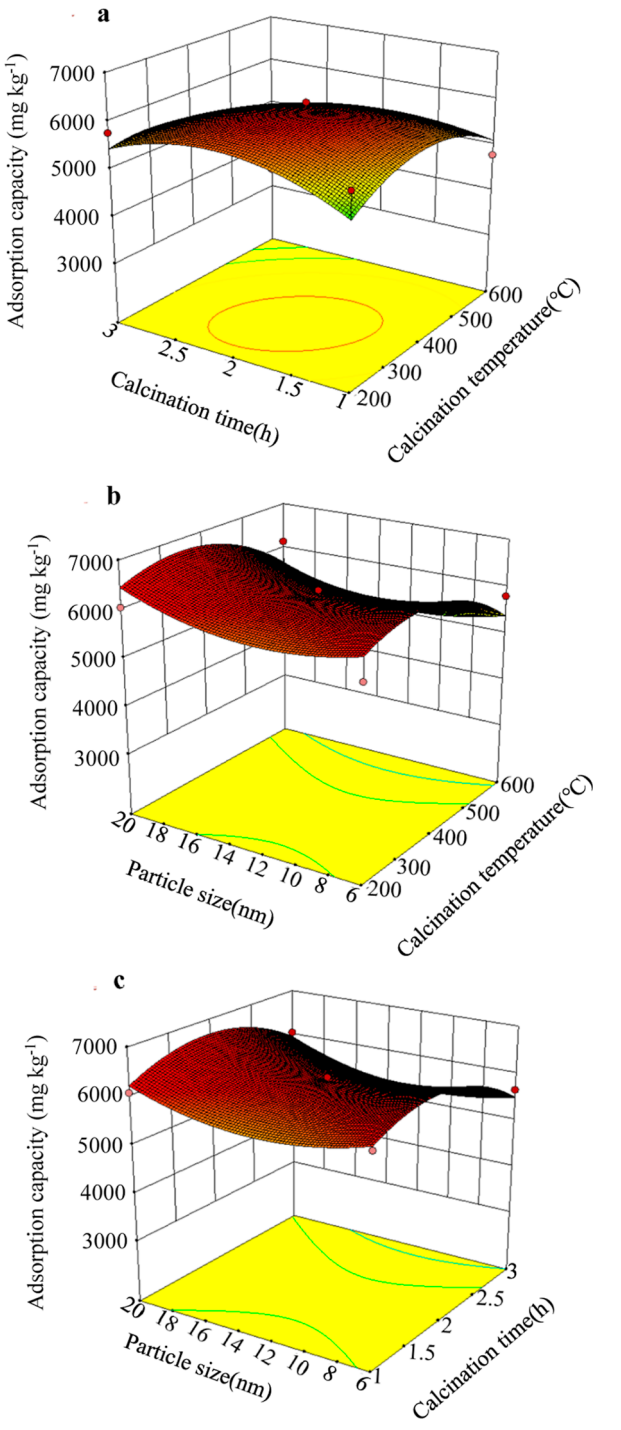

Figure 2. Surface and contour plots of H_2S adsorption capacity versus the interactive effect of particle size, calcination temperature and time. (a), surface and contour of calcination temperature and time versus predicted H_2S adsorption capacity; (b) surface and contour of calcination temperature and particle size versus predicted H_2S adsorption capacity; (c), surface and contour of particle size and calcination time versus predicted H_2S adsorption capacity.

of zeolite did not exhibit obvious damage during calcination, a certain amorphous structure was formed. Similarly, Liu et al.[33] reported that the intensity of the characteristic diffraction peaks gradually decreased with the increasing calcination temperature. Lee et al.[32] showed that Na-A zeolite could transform into nepheline at 800 °C.

https://doi.org/10.1021/acsomega.4c00987
ACS Omega 2024, 9, 19493−19503

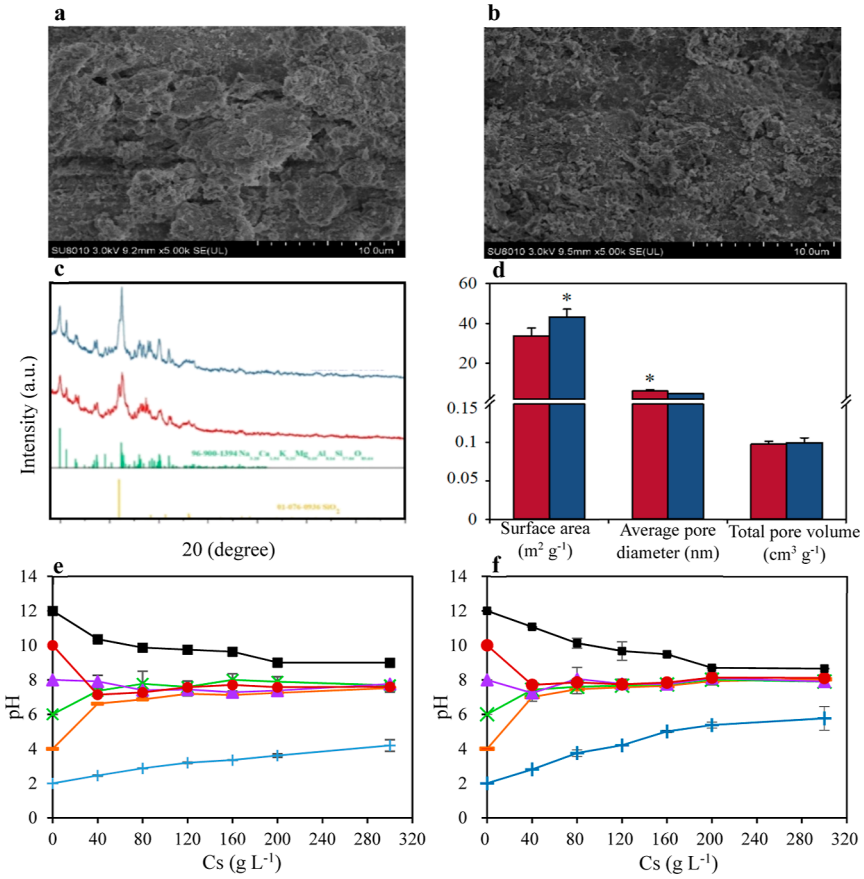

Figure 3. Characteristics of scanning electron micrograph (a,b), XRD pattern (c), surface area and porosity (d), and mass titration curves point of zero net charge (e,f) of the natural zeolite (a,e) and the calcined zeolite (b,f). * means the significant difference at $p < 0.05$.

Compared to the natural zeolite, the specific surface area was lower in the calcined zeolite (Figure 3d). This might be because the crystal structure of the zeolite surface varied with the increasing temperature, thus leading to the collapse of part of the silica−alumina support framework and to the decrease of the specific surface area during calcination.[34] The average pore size increased slightly in the calcined zeolite, but no significant difference was observed in the total pore volume between the natural zeolite and the calcined zeolite, indicating that the pore structure of the zeolite changed after calcination. The collapse of the silica−alumina support framework increased the pore size of the calcined zeolite, which was conducive to the diffusion of H_2S to the interior of the zeolite, and thus increased the adsorption capacity of H_2S. Similarly, Liu et al.[33] reported that the specific surface area of zeolite gradually decreased, and the average pore size gradually increased with the increase of the calcination temperature. This phenomenon was likely due to the dehydration of zeolite at high temperatures, resulting in collapse of the hole wall. Yasyerli et al.[30] found that zeolite became a slight sinter after calcination with an increase of the specific surface area and a decrease of the solid structure. However, Burris and Juenger[35] found that calcination could reduce the specific surface area and total pore volume of the zeolites with increased temperature from 300 to 965 °C, due to the reduction of the porosity of the material. Compared with the natural zeolite, a slightly higher in the average pore diameter and no obvious difference in the total pore volume was observed in the calcined zeolite, which might be attributed to a relatively low calcination temperature of 332 °C used in this study.

The adsorption properties of zeolite are closely related to its surface electrical properties, such as the point of zero charge (pH_{PZC}) and pH_{PZNC}.[36,37] The pH_{PZNC} value refers to the pH value at which the intrinsic surface charge is equal to zero.[36,37] With the increase of the zeolite content, the pH value of the solution moves to the pH_{PZC} value, at which point the surface charge is equal to zero. When the zeolite content reaches a certain value, the pH value of the solution is equal to the pH_{PZC} value, and then, the pH value of the solution is independent of the zeolite content. There is a platform in the mass titration curve, and the corresponding pH value is the pH_{PZC} value of the experimental zeolite. The pH_{PZC} value of the natural zeolite was 7.52−7.76 in this study. This was within the reported pH_{PZC} of natural zeolite in the range of 5.0 to around 7.5.[38] Compared with that of the natural zeolite, the pH_{PZC} value of the calcined zeolite was slightly higher (7.90−8.11) (Figure 3e−f). The higher pH_{PZC} value might be due to Si−OH and Al−OH on the surface and the inner surface of zeolite, which was partly dissociated into Si−O^-, Al−O^-, and H^+ in water and thus decrease the adsorption capacity of acidic H_2S. When the initial pH value was 2, the equilibrium pH value of both the natural zeolite and calcined zeolite gradually increased with the increasing zeolite content, indicating that the H^+ adsorption capacity of the calcined zeolite was higher than that of the natural zeolite. This might be due to that the decrease of crystallinity and the increase of lattice defects increased the contents of the large radius cations, such as Na^+

https://doi.org/10.1021/acsomega.4c00987
ACS Omega 2024, 9, 19493−19503

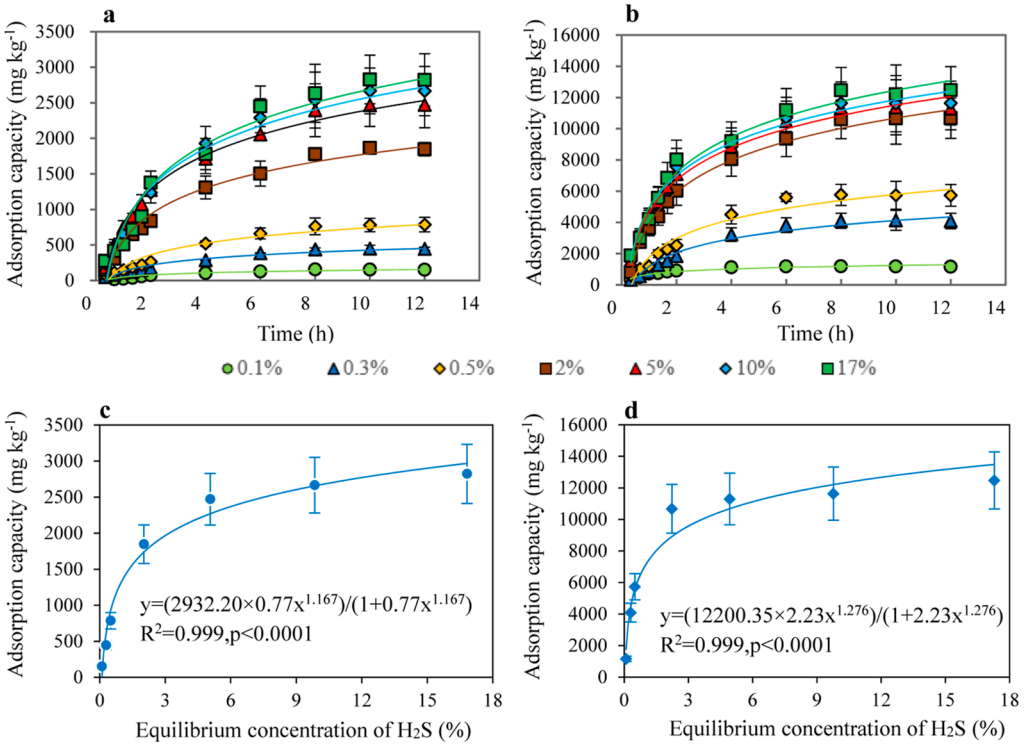

Figure 4. Effect of contact time and concentration in the gaseous phase on the adsorbed amount of H_2S on the natural zeolite (a) and the calcined zeolite (b), and the adsorption of H_2S at T = 303 K on the natural zeolite (c) and the calcined zeolite (d).

and Mg^{2+}, in the calcined zeolite, which could be replaced by H^+.[31]

3.3. Adsorption Isotherm of H_2S. The adsorption isotherms of H_2S on the natural zeolite and the calcined zeolite were investigated under H_2S concentrations of 0.1−17% (v/v) as shown in Figure 4. In the first 2 h, the adsorption capacity of H_2S on the zeolite increased rapidly. With the extension of the reaction time, the adsorption capacity of H_2S on the zeolite increased slowly. As the H_2S concentration increased, the adsorption equilibrium time of the zeolite was increased. At 12 h, the adsorption capacity of H_2S on the zeolite reached saturation at the experimental H_2S concentrations. When the H_2S concentration was higher than 5%, the adsorption capacity of H_2S on the zeolite was close to saturation. The saturation adsorption capacity of H_2S on the natural zeolite and the calcined zeolite was approximately 2653 and 11802 mg kg^{-1}, respectively, indicating that calcination could enhance the saturation adsorption capacity of H_2S on the zeolite. Although the adsorption capacity of H_2S on the calcined zeolite was lower than that on the metal−organic frameworks and modified zeolites reported in the literature (Table 2), it was higher than that on the Al_2O_3/GO composites with graphene oxide addition, zeolite, sepiolite, and molecular sieves (5A and 13X). Moreover, the calcined zeolite is easily obtained and the cost is relatively low.

The gas adsorption of a solid sorbent mainly depends on the interaction between the adsorbent and adsorbate. Many adsorption theories and models have been reported in the literature on the adsorption isotherms of H_2S on zeolites.[54,55] Among them, the Langmuir mode better described the adsorption of H_2S on the experimental zeolites with the high correlation coefficients of 0.999, indicating that the adsorption of H_2S on the zeolite was the formation of a monolayer adsorbate on the outer surface of the adsorbent.

3.4. Desorption and Regeneration of the H_2S-Saturated Zeolite. To estimate whether the H_2S-saturated zeolite can be easily reused, we investigated the regeneration ability of the zeolite. Compared with the calcination temperatures at 200 and 250 °C, the adsorption capacity of H_2S was higher on the regenerated zeolite at 300 and 350 °C (Figure 5). The adsorption capacity of H_2S on the regenerated zeolites was stable and did not vary with the regeneration frequency. When the regeneration temperature was 200−350 °C and the regeneration time was 0.5 h, the adsorbed H_2S could be completely desorbed from the calcined zeolite, and the H_2S adsorption capacity of the regenerated zeolite remained stable. After 9 desorption and regeneration treatments, the adsorption capacity of H_2S could still reach approximately 90% of the initial calcined zeolite, indicating that the calcined regeneration treatment can desorb the adsorbed H_2S without significant damage to the crystal structure of the zeolite. This result might be attributed to the oxidation of H_2S and the lower adsorption capacity of H_2S at high temperatures. Yaşyerli et al.[30] reported that when the adsorption temperature increased from 100 to 600 °C, the adsorption capacity of H_2S on clinoptilolite decreased from 0.087 to 0.03 g g^{-1}. Sigot et al.[49] found that the adsorbed H_2S was poorly desorbed from a 13X zeolite (1.6−2.5 mm beads Siliporite G5 from CECA) in air or helium flow at 350 °C, indicating that H_2S is not physically adsorbed. The amount of desorbed SO_2 was four times higher in the air flow than in the helium flow, which might be due to sulfur oxidation during the desorption process.

3.5. Adsorption Removal of Gas Pollutants by Zeolite. In addition to H_2S, gas pollutants such as CH_3SH, dimethyl disulfide, DMS, toluene, CS_2, CO_2, and CH_4 were also present in the waste gas from the waste treatment plants.[56] The existence of these gas pollutants in the biogas can affect the biogas quality and limit its applications. Here, we

https://doi.org/10.1021/acsomega.4c00987
ACS Omega 2024, 9, 19493−19503

Table 2. Reported Adsorption Capacity of H_2S in Different Adsorbent Materials

materials	gas composition	adsorption capacity	references
metal−organic frameworks, including UiO-66, MOF-801 and Mg-MOF-74	H_2S concentration of 600 mg m^{-3} in N_2 at a flow rate of 30 mL min^{-1}	1.26, 1.25 and 3.81 mg g^{-1} for UiO-66, MOF-801 and Mg-MOF-74, respectively	Yang et al[21]
ZnO	the initial H_2S concentration of 2500−7500 ppmv in heptane	260−700 mg g^{-1}	Zaeri et al[39]
USY zeolite	pressure of 12 bar	126−152 mg g^{-1} at 10−30 °C	Rahmani et al[40]
Al_2O_3/GO composites with graphene oxide addition (0.5−3.0 wt %)	H_2S concentration of 10,000 ppmv	the breakthrough capacity of 0.07−0.43 mg g^{-1}	Hankoy et al[41]
36 all-silica zeolites	the mixed gases of 67% N_2, 18% CO, 14% CO_2, 0.99% H_2O and 0.01% H_2S	78−109 mg g^{-1} at the pore diameter of 7−9 Å	Song et al[42]
NaA nano zeolite	15 ppmv H_2S in N_2 atmosphere at a flow of 100 mL min^{-1}	33.24 mg g^{-1}	Bahraminia et al[43]
zeolite Y and ZSM-5 with Fe_3O_4 nanoparticle	120 ppmv H_2S at 100−300 °C	70 mg g^{-1}	Jafari et al[44]
1.18−1.7 mm NaY zeolite	5 0000 ppmv H_2S in He at 39.9 bar (total pressure)	205−232 mg g^{-1} at 20−40 °C	de Oliveira et al[45]
a silver ion functionalized Cr^{3+} based metal−organic framework	1000 ppmv H_2S in He at a flow rate of 200 mL min^{-1}	97 mg g^{-1}	Pourreza et al[46]
Zn, Co and Ag modified NaX zeolites	2% H_2S, 200 mg m^{-3} COS, 35% CO_2, 63% N_2	43.9, 48.3 and 52 mg g^{-1} for CoX, ZnX and AgX, respectively	Chen et al[47]
rare earth based metal organic frameworks (MOFs) with fcu topology	$CO_2/H_2S/CH_4$ (5%/5%/90%)	28.8−48 mg g^{-1}	Bhatt et al[48]
13X zeolite and an extruded coal-based impregnated activated carbon	4000 ppmv H_2S	142 and 785 mg g^{-1} for zeolite and IAC, respectively	Sigot et al[49]
multilayer graphyne-n (n = 1−3) nanostructures (MGN-n)	pure H_2S	389−485 mg g^{-1}	Lei et al[50]
TiO_2/zeolite	0.1% (1000 ppmv) H_2S at a flow rate 0.02 L min^{-1}	1.6, 2.24 and 4.16 mg g^{-1} for zeolite, TiO_2 and 5-TiO_2/zeolite, respectively	Liu et al[51]
four steam activated carbons (Norit RB1, Norit RBAA1, Norit RGM1 and Desotec Airpel Ultra DS), an impregnated activated alumina (Galipur S), a natural zeolite and a natural sepiolite	200 ppmv H_2S in N_2 at 30 °C	1.71, 20.43, 27.45, 6.60, 1.56, <0.1 and <0.1 mg g^{-1} for Norit RB1, Norit RBAA1, Norit RGM1, Ultra DS, Galipur S, zeolite and sepiolite, respectively	Sisani et al[52]
molecular sieves (5A and 13X) and a natural zeolite (Clinoptilolite)	$CH_4/CO_2/H_2S$ molar composition of 59.95/39.95/0.10	0.5, 1.0 and 1.4 mg g^{-1} for 5A, 13X and clinoptilolite, respectively	Alonso-Vicario et al[53]

https://doi.org/10.1021/acsomega.4c00987
ACS Omega 2024, 9, 19493−19503

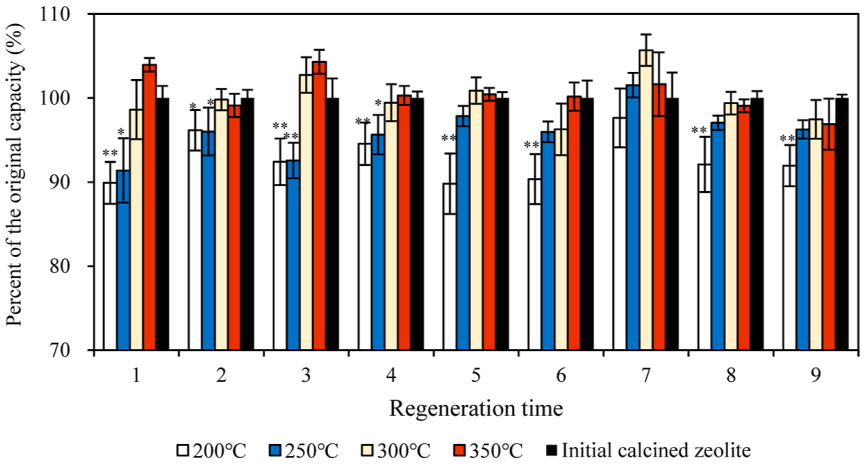

Figure 5. Percent of adsorption capacity of H_2S on the regenerated zeolite to the initial calcined zeolite. * and ** mean the significant difference at $p < 0.05$ and $p < 0.01$, respectively.

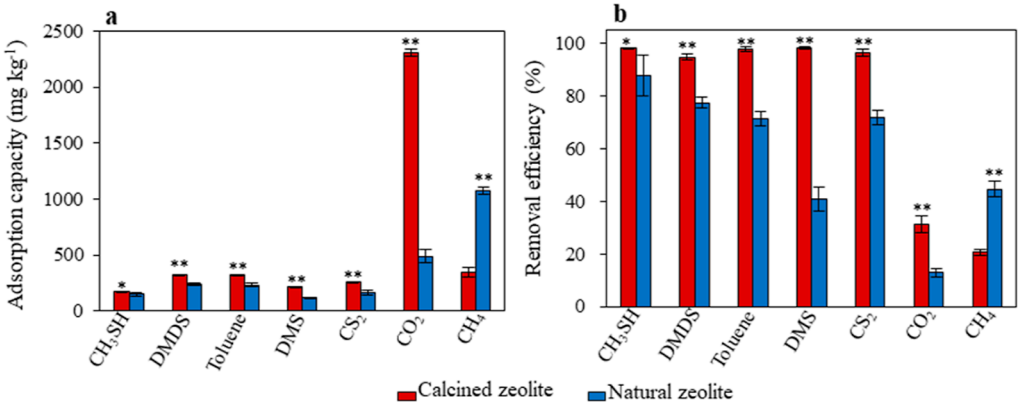

Figure 6. Adsorption capacity (a) and removal efficiency (b) of CH_3SH, DMDS, toluene, DMS, and CS_2 at the concentration of 2000 ppmv, and CO_2 and CH_4 at the concentration of 10% (v/v) on the natural zeolite and the calcined zeolite. * and ** mean the significant difference at $p < 0.05$ and $p < 0.01$, respectively.

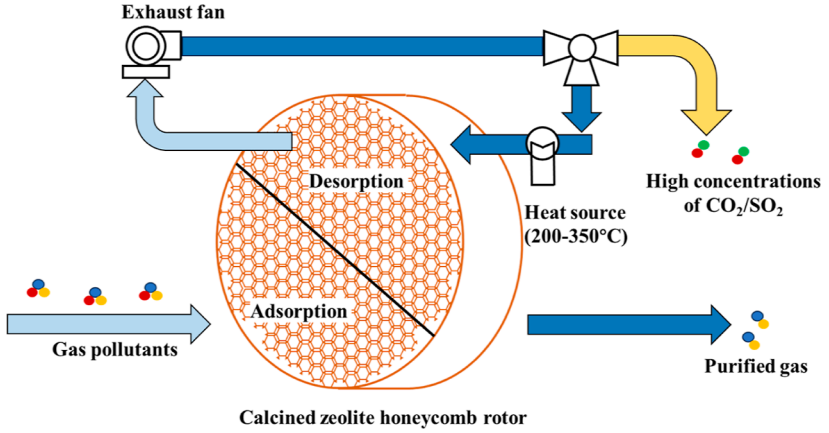

Figure 7. A proposed gas treatment system by a temperature swing adsorption-regeneration process on honeycomb rotors with the calcined zeolites.

investigated the adsorption performances of CH_3SH, dimethyl disulfide (DMDS), DMS, toluene, CS_2, CO_2, and CH_4 on the zeolites. Compared with the natural zeolite, the adsorption capacities of CH_3SH, DMDS, DMS, toluene, CS_2, and CO_2 were significantly higher on the calcined zeolite (Figure 6). The removal efficiencies of CH_3SH, dimethyl disulfide, DMS, toluene and CS_2, reached above 94.7% at the concentration of 2000 ppmv. This result might be because calcination could remove moisture and volatile compounds that exist in the pores and cavities of natural zeolites, and increase the active sites on the surfaces of zeolites.[27]

Compared with H_2S, the adsorption capacity of CO_2 was lower on the zeolite, likely due to the fact that zeolite is a polar material and has a higher adsorption capacity for higher polar

https://doi.org/10.1021/acsomega.4c00987
ACS Omega 2024, 9, 19493−19503

molecules of H_2S than CO_2. A similar result was obtained by Sung et al.[57] who found that the adsorption capacity of H_2S was higher than that of CO_2 on Cu/Ag−Y zeolite. Since the adsorption of zeolite was the formation of a monolayer adsorbate on the outer surface of the adsorbent, the existence of other gases could affect the adsorption capacity of H_2S. Quan et al.[58] reported that the total adsorption amount of zeolite for gas did not change, but the adsorption amount of H_2S was greatly reduced in an adsorption test of mixed gases consisting of CO_2, H_2S and N_2 on the SBA-15 artificial zeolite. Different gases had different effects on the adsorption of H_2S on the zeolite. Weinlaender et al.[59] found that CH_4 had little influence on the adsorption capacity of H_2S on the zeolite, while CO_2 had a greater effect in an adsorption test of mixed gases consisting of CH_4, CO_2, H_2, and O_2 on a Cu-loaded zeolite. This result suggested that high polarity molecular gases had stronger competitive adsorption with H_2S on the zeolite. The adsorption capacity of CH_4 on the calcined zeolite was lower than that of the natural zeolite, which indicated that the calcined zeolite was more conducive to the purification of methane in biogas, natural gas, and landfill gas. Since the calcined zeolite could adsorb various gas pollutants in the waste gas from the waste treatment plants such as CH_3SH, dimethyl disulfide, DMS, toluene, CS_2, CO_2, and CH_4, the coadsorption/competitive effects of multiple pollutants can reduce the adsorption capacity of the calcined zeolite. A cycle between adsorption and regeneration should be optimally operated to remove gas pollutants by the calcined zeolite.

On the basis of the above results, a gas treatment system by a temperature swing adsorption-regeneration process on honeycomb rotors with the calcined zeolites was proposed, as shown in Figure 7. Gas pollutants such as volatile sulfur compounds and volatile organic compounds can pass through the adsorption zone of the zeolite honeycomb rotor with the calcined zeolite as the adsorbent. Gas pollutant molecules can be captured by the calcined zeolite, followed by a desorption process at a temperature of 200−350 °C. The desorbed gases also can be concentrated at the desorption zone by circling gas to high concentrations for further utilization or storage.

4. CONCLUSIONS

The removal performance of H_2S on the calcined zeolite depended on particle size, calcination temperature, and time. Of these parameters, calcination temperature and time had significant influences on the adsorption capacity of H_2S on the zeolite. The optimal calcination conditions for the zeolite were 332 °C, 1.8 h, and 10−20 mm. Calcination could broaden the channels of zeolite, remove the adsorbed gases and impurities, and increase the average pore size and pH_{PZNC} value. The adsorption of H_2S on the zeolite was fitted well with the Langmuir model. The H_2S-saturated zeolite could be easily regenerated at temperatures of 200−350 °C for 0.5 h. In addition to H_2S, the adsorption capacities of CH_3SH, DMDS, DMS, toluene, CS_2, and CO_2 were significantly higher on the calcined zeolite than on the natural zeolite, while the adsorption capacity of CH_4 was lower on the calcined zeolite than on the natural zeolite. Gas pollutants such as volatile sulfur compounds and volatile organic compounds can pass through the adsorption zone of the zeolite honeycomb rotor with the calcined zeolite as the adsorbent. Gas pollutant molecules can be captured by the calcined zeolite, followed by a desorption process at a temperature of 200−350 °C. The desorbed gases also can be concentrated at the desorption zone by circling gas to high concentrations for further utilization or storage. These findings indicated that the calcined zeolite was a cheaper and effective method for removing gas pollutants such as volatile sulfur compounds and volatile organic compounds to purify biogas and to limit toxic concentrations in the working environment.

AUTHOR INFORMATION

Corresponding Author

Ruo He − *Xinjiang Biomass Solid Waste Resources Technology and Engineering Center, College of Chemistry and Environmental Science, Kashi University, Kashi 844000, China; Zhejiang Provincial Key Laboratory of Solid Waste Treatment and Recycling, School of Environmental Science and Engineering, Zhejiang Gongshang University, Hangzhou 310012, China;* orcid.org/0000-0002-2258-1550; Email: heruo@zju.edu.cn

Authors

Xianghao Zha − *Xinjiang Biomass Solid Waste Resources Technology and Engineering Center, College of Chemistry and Environmental Science, Kashi University, Kashi 844000, China*

Feixing Li − *Xinjiang Biomass Solid Waste Resources Technology and Engineering Center, College of Chemistry and Environmental Science, Kashi University, Kashi 844000, China*

Bo Feng − *Xinjiang Biomass Solid Waste Resources Technology and Engineering Center, College of Chemistry and Environmental Science, Kashi University, Kashi 844000, China*

Xin Zhang − *Xinjiang Biomass Solid Waste Resources Technology and Engineering Center, College of Chemistry and Environmental Science, Kashi University, Kashi 844000, China; Zhejiang Provincial Key Laboratory of Solid Waste Treatment and Recycling, School of Environmental Science and Engineering, Zhejiang Gongshang University, Hangzhou 310012, China*

Complete contact information is available at: https://pubs.acs.org/10.1021/acsomega.4c00987

Notes

The authors declare no competing financial interest.

ACKNOWLEDGMENTS

This work was financially supported by Central Guide Local Science and Technology Development of Xinjiang Uygur Autonomous Region with Grants no. ZYYD2023B16 and Open Project Program of Xinjiang Biomass Solid Waste Resources Technology and Engineering Center with Grants no. KSUGCZX202303.

REFERENCES

(1) Jeon, E.; Son, H.; Sa, J. Emission Characteristics and Factors of Selected Odorous Compounds at a Wastewater Treatment Plant. *Sensors* **2009**, *9* (1), 311−326.

(2) Wang, Y.; Fang, J.; Lü, F.; Zhang, H.; He, P. Food waste anaerobic digestion plants: Underestimated air pollutants and control strategy. *Sci. Total Environ.* **2023**, *903*, 166143.

(3) Rincon, C. A.; De Guardia, A.; Couvert, A.; Wolbert, D.; Le Roux, S.; Soutrel, I.; Nunes, G. Odor concentration (OC) prediction based on odor activity values (OAVs) during composting of solid wastes and digestates. *Atmos. Environ.* **2019**, *201*, 1−12.

(4) Plaza, C.; Xu, Q. Y.; Townsend, T.; Bitton, G.; Booth, M. Evaluation of alternative landfill cover soils for attenuating hydrogen sulfide from construction and demolition (C&D) debris landfills. *J. Environ. Manage.* **2007**, *84*, 314−322.
(5) Zhang, L.; Qiu, Y. Y.; Sharma, K. R.; Shi, T.; Song, Y. R.; Sun, J. L.; Liang, Z. S.; Yuan, Z. G.; Jiang, F. Hydrogen sulfide control in sewer systems: A critical review of recent progress. *Water Res.* **2023**, *240*, 120046.
(6) Mansi, M.; Pandey, R.; Ghauri, E. CSR focus in the mission and vision statements of public sector enterprises: evidence from India. *Manag. Audit. J.* **2017**, *32*, 356−377.
(7) Kasperczyk, D.; Urbaniec, K.; Barbusinski, K.; Rene, E. R.; Colmenares-Quintero, R. F. Application of a compact trickle-bed bioreactor for the removal of odor and volatile organic compounds emitted from a wastewater treatment plant. *J. Environ. Manage.* **2019**, *236*, 413−419.
(8) Fajrina, N.; Yusof, N.; Ismail, A. F.; Aziz, F.; Bilad, M. R.; Alkahtani, M. A crucial review on the challenges and recent gas membrane development for biogas upgrading. *J. Environ. Chem. Eng.* **2023**, *11*, 110235.
(9) Shah, M. S.; Tsapatsis, M.; Siepmann, J. I. Hydrogen sulfide capture: from absorption in polar liquids to oxide, zeolite, and metal-organic framework adsorbents and membranes. *Chem. Rev.* **2017**, *117* (14), 9755−9803.
(10) Song, H. X.; Wan, R. H.; Tian, Q. S.; Liu, Y.; Ruan, H. B.; Liu, P.; Wang, Y. Y.; Liu, L. A serial analysis of hydrogen sulfide poisoning: three group accidents. *Forensic Sci. Med. Pathol.* **2023**.
(11) Busca, G.; Pistarino, C. Technologies for the abatement of sulphide compounds from gaseous streams: a comparative overview. *J. Loss Prev. Process Ind.* **2003**, *16* (5), 363−371.
(12) Rattanapan, C.; Boonsawang, P.; Kantachote, D. Removal of H_2S in down flow GAC biofiltration using sulfide oxidizing bacteria from concentrated latex wastewater. *Bioresour. Technol.* **2009**, *100* (1), 125−130.
(13) Milby, T. H.; Baselt, R. C. Hydrogen sulfide poisoning: Clarification of some controversial issues. *J. Ind. Med.* **1999**, *35* (2), 192−195.
(14) Mishra, A.; Kumar, M.; Bolan, N. S.; Kapley, A.; Kumar, R.; Singh, L. Multidimensional approaches of biogas production and up-gradation: Opportunities and challenges. *Bioresour. Technol.* **2021**, *338*, 125514.
(15) Ryckebosch, E.; Drouillon, M.; Vervaeren, H. Techniques for transformation of biogas to biomethane. *Biomass Bioenergy.* **2011**, *35* (5), 1633−1645.
(16) Gui, Y. G.; Chen, J.; Wang, W. B.; Zhu, Y.; Tang, C.; Xu, L. G. Adsorption mechanism of hydrogen sulfide and sulfur dioxide on Au-MoS_2 monolayer. *Superlattices Microstruct.* **2019**, *135*, 106280.
(17) Bouzaza, A.; Laplanche, A.; Marsteau, S. Adsorption-oxidation of hydrogen sulfide on activated carbon fibers: effect of the composition and the relative humidity of the gas phase. *Chemosphere* **2004**, *54* (4), 481−488.
(18) Mescia, D.; Hernandez, S. P.; Conoci, A.; Russo, N. MSW landfill biogas desulfurization. *Int. J. Hydrogen Energy* **2011**, *36* (13), 7884−7890.
(19) Maghsoudi, H.; Soltanieh, M.; Bozorgzadeh, H.; Mohamadalizadeh, A. Adsorption isotherms and ideal selectivities of hydrogen sulfide and carbon dioxide over methane for the Si-CHA zeolite: comparison of carbon dioxide and methane adsorption with the all-silica DD3R zeolite. *Adsorption* **2013**, *19* (5), 1045−1053.
(20) Islamoglu, T.; Chen, Z.; Wasson, M. C.; Buru, C. T.; Kirlikovali, K. O.; Afrin, U.; Mian, M. R.; Farha, O. K. Metal-organic frameworks against toxic chemicals. *Chem. Rev.* **2020**, *120*, 8130−8160.
(21) Yang, Y.; Liu, X.; Yang, C.; Wang, Y.; Wang, H.; Fan, H. Study on the essential features for MOFs to reversible adsorption of H_2S at room temperature. *Colloids Surf., A* **2023**, *674*, 131914.
(22) Abdullah, A. H.; Mat, R.; Somderam, S.; Abd Aziz, A. S.; Mohamed, A. Hydrogen sulfide adsorption by zinc oxide-impregnated zeolite (synthesized from Malaysian kaolin) for biogas desulfurization. *J. Ind. Eng. Chem.* **2018**, *65*, 334−342.
(23) Appel, C.; Ma, L. Q.; Dean Rhue, R.; Kennelley, E. Point of zero charge determination in soils and minerals via traditional methods and detection of electroacoustic mobility. *Geoderma* **2003**, *113*, 77−93.
(24) Chen, M.; Yao, X. Z.; Ma, R. C.; Song, Q. C.; Long, Y. Y.; He, R. Methanethiol generation potential from anaerobic degradation of municipal solid waste in landfills. *Environ. Sci. Pollut. Res.* **2017**, *24* (30), 23992−24001.
(25) Su, Y.; Xia, F. F.; Tian, B. H.; Li, W.; He, R. Microbial community and function of enrichment cultures with methane and toluene. *Appl. Microbiol. Biotechnol.* **2014**, *98* (7), 3121−3131.
(26) Wang, J.; Xia, F. F.; Bai, Y.; Fang, C. R.; Shen, D. S.; He, R. Methane oxidation in landfill waste biocover soil: kinetics and sensitivity to ambient conditions. *Waste Manage.* **2011**, *31* (5), 864−870.
(27) Alonso-Vicario, A.; Ochoa-Gomez, J. R.; Gil-Rio, S.; Gomez-Jimenez-Aberasturi, O.; Ramirez-Lopez, C. A.; Torrecilla-Soria, J.; Dominguez, A. Purification and upgrading of biogas by pressure swing adsorption on synthetic and natural zeolites. *Microporous Mesoporous Mater.* **2010**, *134* (1−3), 100−107.
(28) Yang, Z. X.; Xia, Y. D.; Mokaya, R. Enhanced hydrogen storage capacity of high surface area zeolite-like carbon materials. *J. Am. Chem. Soc.* **2007**, *129* (6), 1673−1679.
(29) Peng, H. G.; Xu, L.; Wu, H. H.; Wang, Z. D.; Liu, Y. M.; Li, X. H.; He, M. Y.; Wu, P. Synthesis and formation mechanism of TS-1@ mesosilica core−shell materials templated by triblock copolymer surfactant. *Microporous Mesoporous Mater.* **2012**, *153*, 8−17.
(30) Yasyerli, S.; Ar, I.; Dogu, G.; Dogu, T. Removal of hydrogen sulfide by clinoptilolite in a fixed bed adsorber. *Chem. Eng. Process.* **2002**, *41* (9), 785−792.
(31) Guo, X. X.; Qiao, L. Y.; Zong, S. S.; Ye, R. P.; He, Y. T.; Cheng, J. K.; Cao, X. Y.; Zhou, Z. F.; Yao, Y. G. Effect of NaY Zeolite at Different Calcination Temperatures on the Activity in Hydroformylation of Formaldehyde. *Chemistry Select* **2022**, *7*, No. e202201574.
(32) Lee, S.; Jang, Y. N.; Bae, I. K.; Chae, S. C.; Ryu, K. W.; Kim, J. K. Adsorption of toxic gases on iron-incorporated Na-A zeolites synthesized from melting slag. *Mater. Trans.* **2009**, *50* (10), 2476−2483.
(33) Liu, X. J.; Yi, D. Z.; Cui, Y. Y.; Shi, L.; Meng, X. Adsorption desulfurization and weak competitive behavior from 1-hexene over cesium-exchanged Y zeolites (CsY). *J. Energy Chem.* **2018**, *27*, 271−277.
(34) Saig, A.; Finkelstein, Y.; Danon, A.; Koresh, J. E. Study of type-A zeolites. Part 2: effect of dehydration on the effective aperture dimension. *J. Phys. Chem. B* **2003**, *107* (48), 13414−13418.
(35) Burris, L. E.; Juenger, M. C. G. Effect of calcination on the reactivity of natural clinoptilolite zeolites used as supplementary cementitious materials. *Constr. Build. Mater.* **2020**, *258*, 119988.
(36) Sposito, G. On points of zero charge. *Environ. Sci. Technol.* **1998**, *32* (19), 2815−2819.
(37) Zhang, H.; Yu, X. J.; Chen, L.; Geng, J. Q. Investigation of radionuclide 63Ni(II) sorption on ZSM-5 zeolite. *J. Radioanal. Nucl. Chem.* **2010**, *286* (1), 249−258.
(38) Eberle, S.; Börnick, H.; Stolte, S. Granular natural zeolites: cost-effective adsorbents for the removal of ammonium from drinking water. *Water* **2022**, *14*, 939.
(39) Zaeri, M. R.; Esmaeilzadeh, F. Hydrogen sulfide removal from normal heptane using zinc oxide, silicon dioxide and zeolite 13X: adsorption capacity, kinetics, selectivity, breakthrough and regeneration. *Environ. Sci. Pollut. Res.* **2023**, *30*, 84314−84333.
(40) Rahmani, M.; Mokhtarani, B.; Rahmanian, N. High pressure adsorption of hydrogen sulfide and regeneration ability of ultra-stable Y zeolite for natural gas sweetening. *Fuel* **2023**, *343*, 127937.
(41) Hankoy, M.; Kitiwan, M.; Phrompet, C.; Ruttanapun, C.; Kaewpengkrow, R.; Vichaphund, S.; Atong, D.; Tunthawiroon, P.

https://doi.org/10.1021/acsomega.4c00987
ACS Omega 2024, 9, 19493−19503

Hydrogen sulfide adsorption on alumina/graphene oxide composites at ambient temperature. *Chiang Mai J. Sci.* **2022**, *49*, 1618−1632.
(42) Song, L.; Du, X.; Chen, Y.; Yang, Z.; Ran, J.; Yang, G.; Shi, Q.; Xue, Z. Screening of zeolites for H_2S adsorption in mixed gases: GCMC and DFT simulations. *Microporous Mesoporous Mater.* **2021**, *328*, 111495.
(43) Bahraminia, S.; Anbia, M.; Koohsaryan, E. Hydrogen sulfide removal from biogas using ion-exchanged nanostructured NaA zeolite for fueling solid oxide fuel cells. *Int. J. Hydrogen Energy* **2020**, *45*, 31027−31040.
(44) Jafari, M. J.; Zendehdel, R.; Rafieepour, A.; Nakhaei Pour, M.; Irvani, H.; Khodakarim, S. Comparison of Y and ZSM-5 zeolite modified with magnetite nanoparticles in removal of hydrogen sulfide from air. *Int. J. Environ. Sci. Technol.* **2020**, *17*, 187−194.
(45) de Oliveira, L. H.; Meneguin, J. G.; Pereira, M. V.; da Silva, E. A.; Grava, W. M.; do Nascimento, J. F.; Arroyo, P. A. H_2S adsorption on NaY zeolite. *Microporous Mesoporous Mater.* **2019**, *284*, 247−257.
(46) Pourreza, A.; Askari, S.; Rashidi, A.; Seif, A.; Kooti, M. Highly efficient SO_3Ag-functionalized MIL-101(Cr) for adsorptive desulfurization of the gas stream: Experimental and DFT study. *Chem. Eng. J.* **2019**, *363*, 73−83.
(47) Chen, X.; Shen, B.; Sun, H.; Zhan, G. Ion-exchange modified zeolites X for selective adsorption desulfurization from Claus tail gas: Experimental and computational investigations. *Microporous Mesoporous Mater.* **2018**, *261*, 227−236.
(48) Bhatt, P. M.; Belmabkhout, Y.; Assen, A. H.; Weselinski, L. J.; Jiang, H.; Cadiau, A.; Xue, D. X.; Eddaoudi, M. Isoreticular rare earth fcu-MOFs for the selective removal of H_2S from CO_2 containing gases. *Chem. Eng. J.* **2017**, *324*, 392−396.
(49) Sigot, L.; Ducom, G.; Germain, P. Adsorption of hydrogen sulfide (H_2S) on zeolite (Z): retention mechanisn. *Chem. Eng. J.* **2016**, *287*, 47−53.
(50) Lei, G.; Liu, C.; Li, Q.; Xu, X. Graphyne nanostructure as a potential adsorbent for separation of H_2S/CH_4 mixture: Combining grand canonical Monte Carlo simulations with ideal adsorbed solution theory. *Fuel* **2016**, *182*, 210−219.
(51) Liu, C.; Zhang, R.; Wei, S.; Wang, J.; Liu, Y.; Li, M.; Liu, R. Selective removal of H_2S from biogas using a regenerable hybrid TiO_2/zeolite composite. *Fuel* **2015**, *157*, 183−190.
(52) Sisani, E.; Cinti, G.; Discepoli, G.; Penchini, D.; Desideri, U.; Marmottini, F. Adsorptive removal of H_2S in biogas conditions for high temperature fuel cell systems. *Int. J. Hydrogen Energy* **2014**, *39*, 21753−21766.
(53) Alonso-Vicario, A.; Ochoa-Gomez, J. R.; Gil-Rio, S.; Gomez-Jimenez-Aberasturi, O.; Ramirez-Lopez, C. A.; Torrecilla-Soria, J.; Dominguez, A. Purification and upgrading of biogas by pressure swing adsorption on synthetic and natural zeolites. *Microporous Mesoporous Mater.* **2010**, *134*, 100−107.
(54) Abdul Kareem, F. A.; Shariff, A. M.; Ullah, S.; Dreisbach, F.; Keong, L. K.; Mellon, N.; Garg, S. Experimental measurements and modeling of supercritical CO_2 adsorption on 13X and 5A zeolites. *J. Nat. Gas Sci. Eng.* **2018**, *50*, 115−127.
(55) Starke, A.; Pasel, C.; Bläker, C.; Eckardt, T.; Zimmermann, J.; Bathen, D. Investigation of the Adsorption of Hydrogen Sulfide on Faujasite Zeolites Focusing on the Influence of Cations. *ACS Omega* **2022**, *7*, 43665−43677.
(56) Yao, X. Z.; Ma, R. C.; Li, H. J.; Wang, C.; Zhang, C.; Yin, S. S.; Wu, D. L.; He, X. Y.; Wang, J.; Zhan, L. T.; He, R. Assessment of the major odor contributors and health risks of volatile compounds in three disposal technologies for municipal solid waste. *Waste Manage.* **2019**, *91*, 128−138.
(57) Sung, C. Y.; Al Hashimi, S.; McCormick, A.; Cococcioni, M.; Tsapatsis, M. A DFT study on multivalent cation-exchanged Y zeolites as potential selective adsorbent for H_2S. *Microporous Mesoporous Mater.* **2013**, *172*, 7−12.
(58) Quan, W. Y.; Wang, X. X.; Song, C. S. Selective removal of H_2S from biogas using solid amine-based "molecular basket" sorbent. *Energy Fuel* **2017**, *31* (9), 9517−9528.
(59) Weinlaender, C.; Neubauer, R.; Hauth, M.; Hochenauer, C. Removing H_2S from biogas using sorbents for solid oxide fuel cell applications. *Chem. Ing. Tech.* **2017**, *89* (9), 1247−1254.

https://doi.org/10.1021/acsomega.4c00987
ACS Omega 2024, 9, 19493−19503